BIOCHEMISTRY
including biophysical chemistry & molecular biology

Article

pubs.acs.org/biochemistry

Role of Positively Charged Residues of the Second Transmembrane Domain in the Ion Transport Activity and Conformation of Human Uncoupling Protein-2

Tuan Hoang,[†,§] Tijana Matovic,[†] James Parker,[†] Matthew D. Smith,[‡,§] and Masoud Jelokhani-Niaraki*[,†,§]

[†]Department of Chemistry and Biochemistry and [‡]Department of Biology, Wilfrid Laurier University, Waterloo, Ontario N2L 3C5, Canada

[§]Biophysics Interdepartmental Group, University of Guelph, Guelph, Ontario N1G 2W1, Canada

Supporting Information

ABSTRACT: Residing at the inner mitochondrial membrane, uncoupling protein-2 (UCP2) mediates proton transport from the intermembrane space (IMS) to the mitochondrial matrix and consequently reduces the rate of ATP synthesis in the mitochondria. The ubiquitous expression of UCP2 in humans can be attributed to the protein's multiple physiological roles in tissues, including its involvement in protective mechanisms against oxidative stress, as well as glucose and lipid metabolisms. Currently, the structural properties and ion transport mechanism of UCP2 and other UCP homologues remain poorly understood. UCP2-mediated proton transport is activated by fatty acids and inhibited by di- and triphosphate purine nucleotides. UCP2 also transports chloride and some other small anions. Identification of key amino acid residues of UCP2 in its ion transport pathway can shed light on the protein's ion transport function. On the basis of our previous studies, the second transmembrane helix segment (TM2) of UCP2 exhibited chloride channel activity. In addition, it was suggested that the positively charged residues on TM2 domains of UCPs 1 and 2 were important for their chloride transport activity. On this basis, to further understand the role of these positively charged residues on the ion transport activity of UCP2, we recombinantly expressed four TM2 mutants: R76Q, R88Q, R96Q, and K104Q. The wild type UCP2 and its mutants were purified and reconstituted into liposomes, and their conformation and ion (proton and chloride) transport activity were studied. TM2 Arg residues at the matrix interface of UCP2 proved to be crucial for the protein's anion transport function, and their absence resulted in highly diminished Cl^- transport rates. On the other hand, the two other positively charged residues of TM2, located at the UCP2−IMS interface, could participate in the salt-bridge formation in the protein and promote the interhelical tight packing in the UCP2. Absence of these residues did not influence Cl^- transport rates, but disturbed the dense packing in UCP2 and resulted in higher UCP2-mediated proton transport rates in the presence of long chain fatty acids. Overall, the outcome of this study provides a deeper and more detailed molecular image of UCP2's ion transport mechanism.

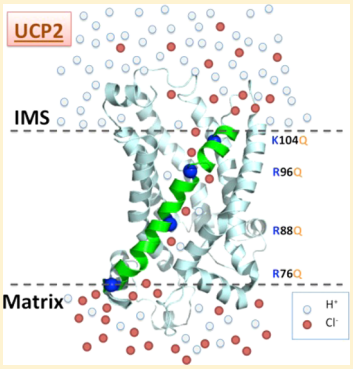

Located in the inner mitochondrial membrane (IMM), uncoupling proteins (UCPs) dissipate the proton gradient across the inner membrane and, consequently, uncouple oxidative phosphorylation from ATP synthesis in the mitochondria.[1,2] Five human UCPs have been identified with different expression patterns.[2,3] UCP1, the prototypical UCP, was originally found in brown adipose tissues (BAT), and its proton transport activity plays an important role in heat generation in these tissues.[1,2,4] Among all UCP homologues, UCP2 is unique in its ubiquitous expression.[1−3] UCP2 shares 59% sequence identity with UCP1 and has been shown to have comparable proton transport activity.[5] The wide tissue distribution of UCP2 suggests that it plays important physiological and even pathological roles. For instance, the effect of UCP2-mediated proton transport in diminishing mitochondrial oxidative stress has been well studied.[2,3,6] Other studies on the physiological roles of UCP2 include the expression of this protein in β-cells and its role in glucose homeostasis in the pancreas.[1,3,7] Belonging to the mitochondrial carrier family (MCF), UCP2 and other UCPs share a similar 3-fold pseudosymmetry in the protein topology.[1,8,9] The amino acid sequence of UCP2 consists of three repeated domains, each of which is comprised of two transmembrane (TM) segments that are connected by an amphipathic helix loop. Each repeat consists of a signature motif Px[D/E]xx[K/R]x[R/K]-20−30 residues-[D/E]Gxxxx[W/Y/F]-[K/R]G spanning from the odd-numbered TMs (1, 3, and 5) to the end of the matrix loops connecting to the even-numbered TMs (2, 4, and 6).[1,8,9] Recently, the structure of UCP2 was studied using the NMR fragment searching method[9] (Figure 1). In sharing many structural similarities with the ADP/ATP carrier (AAC), the predicted three-dimensional (3-D) structure for UCP2 resembles a funnel-like carrier or channel.[9]

Received: January 4, 2015
Revised: March 18, 2015
Published: March 19, 2015

DOI: 10.1021/acs.biochem.5b00177
Biochemistry 2015, 54, 2303−2313

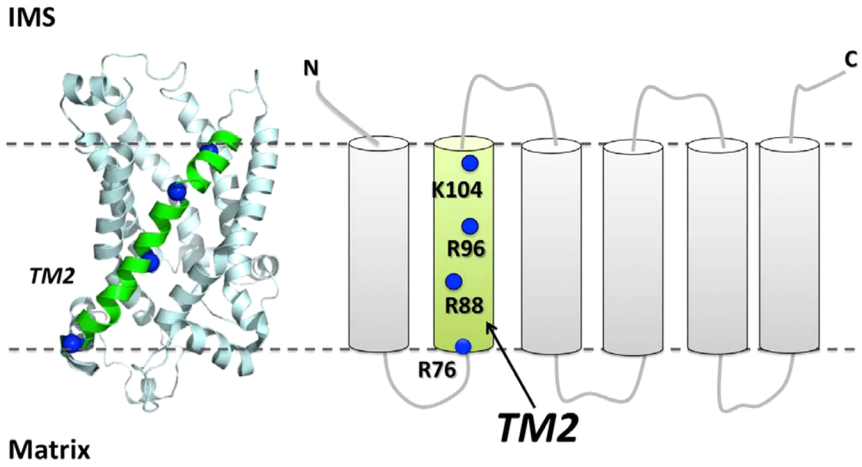

Figure 1. Design of UCP2-TM2 mutants. The 3-D structure of UCP2 (PDB ID: 2LCK) solved by NMR fragment searching is depicted on the left.[9] The second transmembrane domain (TM2) is highlighted in green, and the locations of the positively charged residues that were mutated in this study (R76, R88, R96, K104) are highlighted with blue balls. On the right, the topology of UCP2 in the inner mitochondrial membrane is shown using the same color scheme. Both N- and C-termini of UCP2 are located in the IMS.

Table 1. Primers Used for Overlap Extension PCR To Generate UCP2 Point Mutants[a]

mutant	primer name	primers
flanking primers	Sense 1 (A) (NdeI) 5′=CC*CATATG*	5′-CCCATATGGTTGGGTTCAAGGCCACAGATG-3′
	Antisense 2 (D) (HindIII) 5′=CC*AAGCTT*	5′-CCAAGCTTTTAGAAGGGAGCCTCTCGGG-3′
R76Q	Antisense (B)	5′-GCCCATTGTAGAGGCTCTGGGGGCCCTCAGTACG-3′
	Sense (C)	5′-CGTACTGAGGGCCCCCAGAGCCTCTACAATGGGC-3′
R88Q	Antisense (B)	5′-GGCAAAGCTCATTTGCTGCTGCAGGCCGGCAAC-3′
	Sense (C)	5′-GTTGCCGGCCTGCAGCAGCAAATGAGCTTTGCC-3′
R96Q	Antisense (B)	5′-CATACAGGCCGATCTGGACAGAGGCAAAGCTC-3′
	Sense (C)	5′-GAGCTTTGCCTCTGTCCAGATCGGCCTGTATG-3′
K104Q	Antisense (B)	5′-CTTGGTGTAGAACTGCTGGACAGAATCATACAGGCC-3′
	Sense (C)	5′-GGCCTGTATGATTCTGTCCAGCAGTTCTACACCAAG-3′

[a]All primers were purchased from Invitrogen. The restriction sites were italicized. The three-base codes corresponding for the point mutation were underlined.

Although the proton transport activity of UCP2 and other UCPs has been observed in many studies, the mechanism of transport is poorly understood. It is acknowledged that UCP-mediated proton transport is activated by fatty acids (FAs) and inhibited by purine nucleotides (ATP, ADP, GTP, and GDP).[1,2] Two hypotheses have been suggested to explain the FA-activated UCP-mediated proton transport, using UCP1 as the prototypic UCP.[1,2] In the FA-cycling model, protonated FAs flip-flop across the lipid bilayers and release protons into the matrix due to the pH difference, and the resulting FA anions are transported back through UCPs.[1,10,11] In the cofactor model, FA carboxyl groups can buffer protons and enhance the rate of proton movement through UCPs.[1,8,12] Studies supporting or opposing each hypothesis also consider the anion (chloride, bromide, fatty acid anions) transport activity of UCP1 and other UCPs as one of the main argument points, which in some cases result in contradictory interpretations.[8,13,14] Specifically, on one hand the lower chloride transport rate of UCP supports the idea that proton and anion transport pathways could be distinct. On the other hand, retardation in proton transport rates by fatty acid anions could support overlapping of these transport pathways. In addition, the mode of transport of anions (carrier vs channel) is still debated. In one study, hamster UCP1 exhibited the properties of a voltage-dependent anion channel, where mutation of both conserved Arg residues in TM2 (R83 and R91) led to the inactivation of the protein's Cl^- transport activity.[14] In another study, direct patch-clamp measurements of UCP1 from the IMM of BAT mitochondria showed that UCP1 can transport both protons and anions.[15] With a high sequence identity between UCP1 and UCP2 (59%), it is expected that these proteins have comparable ion transport activities.[1] In fact, all six TM peptide segments of UCP2 were chemically synthesized, and chloride channel activity that was comparable to the chloride channel activity of hamster UCP1 was observed for TM2.[14,16] In addition, mutation of conserved positively charged residues on the TM2 of UCP2, R88, and R96, resulted in unstable channel activities.[16] Thus, we have suggested previously that the TM2 of UCP2 can play an important role in the protein's ion transport pathway.[16]

In the current study, to understand the role of the four positively charged residues, located on the TM2 of UCP2, in the protein's ion transport activity, we prepared four UCP2 mutants via site-directed mutagenesis (Figure 1). Human UCP2 and its single mutants were recombinantly expressed, purified, and reconstituted into liposomes for conformational and ion transport studies. Our results suggest that two Arg residues, located close to the matrix side of the membrane are crucial for UCP2-mediated anion transport. We also investigated the impact of the FA hydrocarbon chain length on activating UCP2-mediated proton transport. The results from this study offer deeper insights into the mechanism of the ion

DOI: 10.1021/acs.biochem.5b00177
Biochemistry 2015, 54, 2303−2313

transport activity of UCP2 and the protein's structure−function relationship.

EXPERIMENTAL PROCEDURES

UCP2 Construct and Chemicals. The human UCP2 cDNA clone (pET21a-UCP2) was a gift from Dr. Martin Brand (MRC Dunn Human Nutrition Unit, Cambridge, UK). All designed primers for mutagenesis experiments were purchased from Invitrogen (Thermo Fisher Scientific, Waltman, MA). Restriction enzymes were from New England BioLabs (Ipswich, MA). Egg yolk L-α-lecithin (Sigma, St. Louis, MO) contained at least 60% phosphatidylcholine by weight. The remaining 40% comprised mostly phosphatidylethanolamine and other lipids. C_8E_4 (octyltetraoxyethylene) was obtained from Bachem (Torrance, CA). Triton X-100 (TX-100), Triton X-114 (TX-114), and sarcosyl (*N*-lauroyl-sarcosine, sodium salt) were from Calbiochem-EMD Biosciences (Gibbstown, NJ). The fluorescent probe 6-methoxy-*N*-(3-sulfopropyl)-quinolinium (SPQ) (99%) was from Biotium (Burlington, ON). All other chemicals were from Sigma.

Site-Directed Mutagenesis. Four cDNAs encoding mutant versions of UCP2 containing single point mutations were generated using site-directed mutagenesis. The proteins encoded by the mutated cDNAs, denoted R76Q, R88Q, R96Q, and K104Q, contained single point mutations in the TM2 domain (Figure 1). The mutations were incorporated into the cDNAs using overlap extension PCR.[17] Specifically, the wild type human UCP2 cDNA in pET21a vector was used as the template to generate two overlapping fragments of the cDNA using mutagenic primers.[18] The mutagenic and flanking primers used to generate all four mutants are shown in Table 1 (note that the same flanking primers were used in all cases). Briefly, one of the overlapping PCR products was generated using flanking primer A and mutagenic primer B. The second PCR product was generated using mutagenic primer C and flanking primer D. The resulting cDNA fragments containing the mutation were purified and used as templates for a third PCR reaction together with flanking primers A and D. The product of this reaction was then digested by restriction enzymes (NdeI and *Hin*dIII), ligated into pET21a vector, and transformed into *Escherichia coli* DH5α using standard techniques. The four resulting constructs, pET21a:UCP2-R76Q, pET21a:UCP2-R88Q, pET21a:UCP2-R96Q, and pET21a:UCP2-K104Q, encode mutant versions of UCP2 containing single point mutations in the TM2, denoted UCP2-R76Q, UCP2-R88Q, UCP2-R96Q, and UCP2-K104Q, respectively. DNA sequencing (TCAG, Hospital for Sick Children, Toronto, ON) was used to confirm the identity of each mutant.

Overexpression of UCP2 Mutants. Constructs encoding wild type and mutant versions of recombinant UCP2 were transformed into one of two protein expression strains of *E. coli*. Specifically, pET21a:UCP2-WT, pET21a:UCP2-R76Q, and pET21a:UCP2-R88Q were transformed into *E. coli* BL21-(DE3), whereas pET21a:UCP2-R96Q and pET21a:UCP2-K104Q were transformed into *E. coli* C43(DE3). Protein overexpression was achieved after induction with 0.8 mM isopropyl β-D-thiogalactoside (IPTG) for 4 h at 22 °C.

Extraction and Refolding of Recombinant Versions of UCP2. The extraction, purification, refolding, and reconstitution of WT and mutant versions of UCP2 were achieved as described previously,[18] with minor modifications. Following overexpression, bacterial cell pellets were collected at 8000*g* for 15 min (4 °C) and resuspended in extraction buffer (500 mM NaCl, 20 mM Tris-HCl, pH 8.0). The cells were lysed using 200 μg/mL lysozyme (4 °C, 30 min) (followed by probe-tip sonication). The cell lysates were centrifuged at 48556*g* (TLA-100.3 rotor, Beckman-Coulter) for 15 min at 4 °C to yield pellets containing the inclusion bodies (IBs). The IBs were washed stepwise with 2 M urea, 3% Triton X-100, 1% LDAO, and 0.1% sarcosyl in extraction buffer. The final pellets were dissolved in 2% sarcosyl in buffer A [50 mM CAPS, 25 mM DTT, 2 mM PMSF, 1 mM ATP, and 10% glycerol, pH 10.0] for 2 h at 4 °C. The mixture was centrifuged at 14000*g* for 10 min (4 °C), and insoluble particles were removed. The supernatant was diluted with buffer B [1% Triton X-114, 10% glycerol] in a 4:6 volumetric ratio. After a 2 h incubation at 4 °C, the ∼10-mL mixture was dialyzed three times against 500 mL of buffer A mixed with buffer B in a 4:6 ratio (A:B) to remove sarcosyl and small contaminants. The dialyzed mixture was supplemented with 5 mg/mL L-α-lecithin and 1 mM ATP and concentrated ∼2-fold using an Ultrafree-15 centrifugal filter device (Millipore). The final protein purity was analyzed by SDS-PAGE, and the protein concentrations were determined using a Lowry-based protein assay (Bio-Rad, Hercules, CA) (typical concentrations were ∼10−15 mg/mL).

Western Blot Analysis. The identities of the recombinant UCP2 proteins extracted from IBs were confirmed by Western blot analysis. Briefly, 10−50 μg of total protein was run on a 12% SDS-PAGE gel and transferred (110 min, 15 V) to nitrocellulose membranes using the semidry technique. The membranes were stained with Amido Black to confirm the efficiency of transfer and were blocked overnight at 4 °C using TBS-buffer containing 5% (w/v) skim milk and 0.05% Tween-20. To confirm the presence of UCP2, Rabbit IgG anti-UCP1/2/3 (Santa Cruz Biotechnology Inc.) was used as the primary antibody (1:2000 dilution). Goat peroxidase-conjugated antibody raised against rabbit (Rockland) was used as the secondary antibody (1:4000 dilution). Immunodetection was achieved by luminescence with ECL Western Blot reagent (GE Healthcare), and an image was captured using a Bio-Rad VersaDoc (MP4000) Imaging System.

Reconstitution of UCP2-WT and Mutants into Liposomes. The reconstitution of purified proteins into liposomes for spectroscopic and ion transport studies was previously described.[18] Briefly, dissolved lipid L-α lecithin in chloroform was dried overnight under vacuum and rehydrated in the reconstitution buffer. Multilamellar phospholipid was solubilized in the detergent C_8E_4 at a detergent/lipid ratio of 2.5/1 (w:w). Purified proteins were added to this lipid−detergent mixed micelle solution. For the ion transport assays, the fluorescent probe SPQ was included in the internal buffer entrapped inside the liposomes at a concentration of 3 mM. Protein-free liposome controls were prepared in parallel for all experiments. In all cases, liposomes/proteoliposomes were formed spontaneously following detergent removal using SM-2 Biobeads (Bio-Rad). The external SPQ probe was removed using a coarse Sephadex G25-300 (GE Healthcare) spin column. The protein was reconstituted with no preference for one orientation over the other, as discussed previously.[18]

CD and Fluorescence Spectroscopic Measurements. Far-UV CD spectra were measured in a 0.1 cm-path length quartz cell on an Aviv 215 spectropolarimeter (Aviv Biomedical, NJ). Ellipticities are reported as mean residue ellipticities, $[\theta]$. Secondary structure content of proteins was estimated from backbone CD spectra using the deconvolution program CDSSTR, and the analysis was based on a set of 48

DOI: 10.1021/acs.biochem.5b00177
Biochemistry 2015, 54, 2303−2313

reference proteins and performed on the Dichroweb Web site.[19,20] Steady-state fluorescence measurements were performed using a Cary Eclipse spectrophotometer (Varian, CA). Excitation and emission bandwidth slits for all measurements were 5 nm, and a scan speed of 600 nm/min was used throughout all experiments (25 °C).

Proton and Chloride Transport Measurements. Proton and chloride transport assays for reconstituted UCPs were described in our previous study.[18] Briefly, 40 μL of proteoliposomes/liposomes entrapping ~3 mM SPQ was added to 1.96 mL of external buffer. The internal buffer for proton transport assays contained 30 mM TES, 80 mM TEA_2SO_4, and 1 mM EDTA. The external buffer for these assays contained 30 mM TES, 80 mM K_2SO_4, and 1 mM EDTA. In the chloride transport experiments, the internal buffer consisted of 10 mM sodium phosphate, 133 mM TEA_2SO_4, and 1 mM EDTA, and the external buffer contained 10 mM sodium phosphate, 200 mM KCl, and 1 mM EDTA. All media were kept constant at pH 7.2. Both ion (proton and chloride) transport activities mediated by UCP2 were initiated by triggering K^+ influx using the K^+-ionophore valinomycin. In the case of the chloride transport assay, chloride ions, whose influx was mediated through UCP2, collisionally quenched SPQ fluorescence. In the case of the proton transport assay, FAs were added to a final concentration of 100 μM to activate UCP-mediated H^+ efflux. Three FAs varying in hydrocarbon lengths were compared in this study: lauric acid (LA) (C_{12} chain), myristic acid (MA) (C_{14} chain), and palmitic acid (PA) (C_{16} chain). UCP2-mediated proton efflux resulted in the deprotonation of TES buffer in the internal medium; TES anions quenched the SPQ fluorescence. All ion transport data were corrected by subtraction from the nonspecific ion leak and calibrated for SPQ fluorescence response and internal volume of liposomes/proteoliposomes, as described previously.[18] The proton transport of reconstituted UCP2 proteins was fully inhibited by ATP (one of its physiological inhibitors) at the concentration of 100 mM, as reported previously.[18] The proteoliposomes retained their integrity and stability in the presence of FAs, valinomycin, or purine nucleotides.

Amino Acid Sequence Analysis and Structural Modeling of UCP2 Mutants. Protein primary sequence alignment of UCPs and AAC were performed using Clustal Omega.[21] Protein sequence alignment analysis was viewed through Jalview program.[22] The 3-D structural model of UCP2 (PDB ID: 2LCK) was viewed using Pymol.[9,23] Electrostatic potential was calculated using the Poisson−Boltzmann solver (APBS), with pH = 7.2 and a salt concentration of 150 mM.[24−26]

Statistical Analysis. Data were analyzed using the one-way analysis of variance (ANOVA) statistical method. A p of <0.05 was considered statistically significant.

RESULTS

Expression, Purification, and Reconstitution of Wild Type and Mutant Versions of UCP2 into Liposomes. cDNAs encoding mutant versions of UCP2 were generated using overlap extension PCR, and recombinant versions of the wild type and mutant proteins were expressed in *E. coli*. We were able to obtain each version of recombinant UCP2 in high yield (~10−15 mg/mL) and high purity after extraction from inclusion bodies (Figure 2A). Western Blot analysis using anti-UCP1/2/3 antibody confirmed the presence of UCP2 (wild type and mutants) in the bacterial inclusion bodies (Figure 2B).

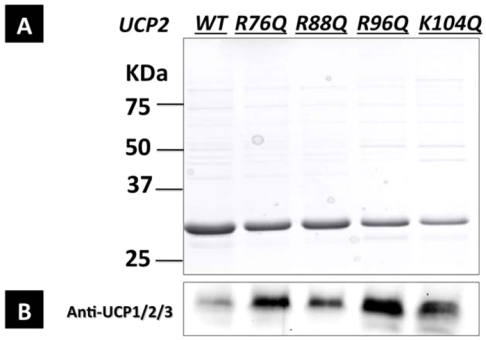

Figure 2. Expression and purification of recombinant wild type and mutant forms of UCP2. (A) SDS-PAGE analysis of purified recombinant UCP2-WT, -R76Q, -R88Q, -R96Q, and -K104Q from inclusion bodies stained with Coomassie Brilliant Blue. Molecular weight markers (kDa) are indicated on the left. (B) Western Blot detection of recombinant UCP2 proteins using anti-UCP1/2/3, detected by chemiluminescence using a horseradish peroxidase-linked secondary antibody.

These purified proteins were subsequently reconstituted into liposomes for further analysis.

The structure and ion transport activities of UCP2 and its mutants were studied in their reconstituted forms in egg yolk L-α-lecithin bilayers. Protein conformation was monitored by CD and fluorescence spectroscopies for each reconstituted protein. An increase in molar ellipticity in the far-UV CD spectrum of UCP2-WT after reconstitution into liposomes as compared to mixed detergent/lipid micelles indicates that UCP2 secondary structure was enhanced (Figure 3A). The CD spectrum of the reconstituted UCP2 indicates a relatively high α-helical content of the protein in liposomes (Figure 3A). Specifically, the far-UV CD spectrum of UCP2 in L-α-lecithin vesicles contained a local negative maximum at ~220 nm, a negative shoulder at ~210 nm and a positive maximum at ~193 nm (Figure 3A). Deconvolution of this CD spectrum revealed that the reconstituted protein contained ~32% helical content. It is important to note that the CD spectra of proteins reconstituted in liposome systems could be distorted due to the light scattering-induced flattening effect.[27] This possible artifact was also noted in our previous study and could cause a lower positive ellipticity of the CD spectra, resulting in an underestimation of helical content.[28] The reconstituted WT and mutant UCP2 proteins contained no trace of detergents that could interfere with the ion transport assays. This is shown in Figure 3B, where UCP2 (and its mutants) in detergent/lipid mixed micelles exhibited a high fluorescence intensity at ~305 nm (λ_{ex} = 280 nm) due to the presence of TX-114 (Figure 3B, inset). In comparison, the reconstituted UCP2 (and its mutants) showed a drastic decrease in the fluorescence signal, together with a red shift of λ_{max} toward 340 nm, which accounts for the intrinsic fluorophores (Phe, Tyr, and Trp) present in the protein (Figure 3B).

Proton and Chloride Transport Rates of UCP2-WT and Mutants. The ion transport ability of UCP2-WT and the mutants were analyzed using SPQ fluorescence quenching assays as described previously (Figure 3C,D).[18] The proton and chloride fluxes of proteins were measured within the first 30 s after the addition of valinomycin. The UCP2-containing proteoliposomes (and protein-free liposome controls) were stable for 6−8 h during the fluorescence quenching assays. As shown in Figure 4, wild type UCP2 and its mutants transported

DOI: 10.1021/acs.biochem.5b00177
Biochemistry 2015, 54, 2303−2313

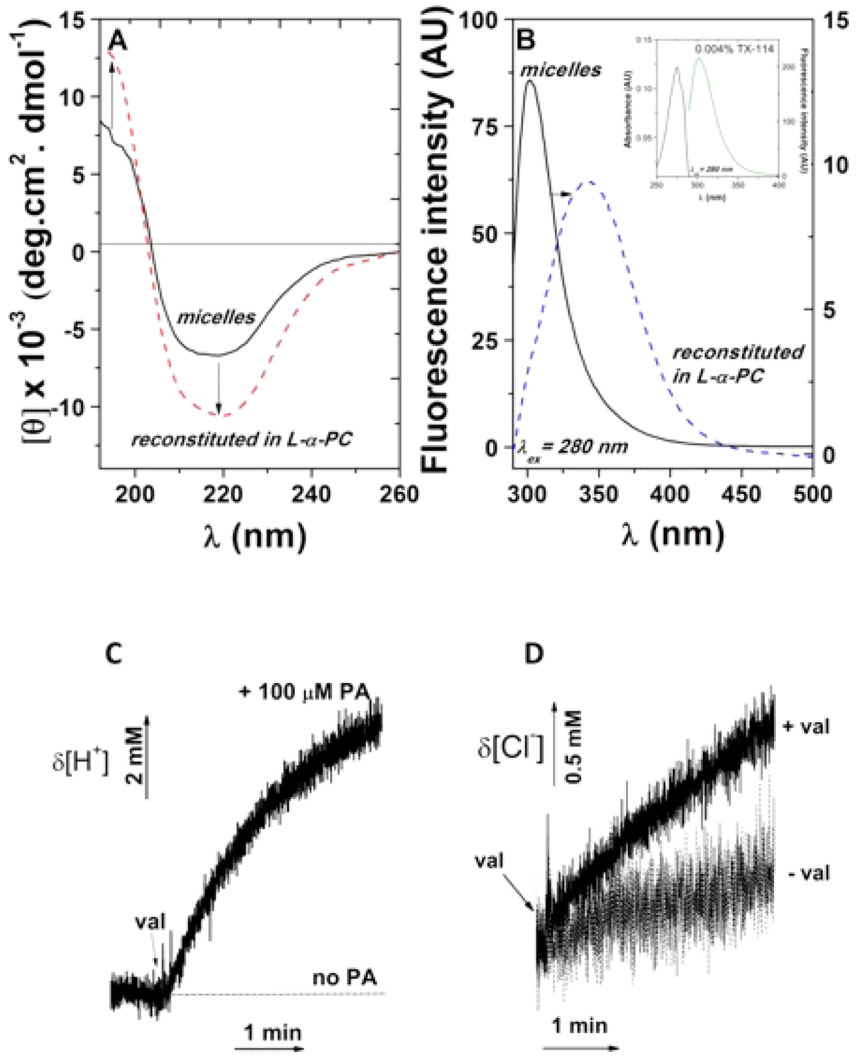

Figure 3. Reconstitution of UCP2-WT into egg yolk L-α-lecitin liposomes. (A) Comparative far-UV CD spectra of UCP2-WT in mixed detergents/lipids micelles (before reconstitution) and in L-α-lecithin vesicles (after reconstitution). Protein and lipid concentrations were ~1 μM and 1 mM, respectively. All samples were measured in 10 mM potassium phosphate buffer, pH 7.2, using a 0.1 cm path length quartz cuvette. The reported spectra are an average of at least eight scans. (B) Comparative fluorescence spectra (λ_{ex} = 280 nm) of UCP2-WT in mixed detergent/lipid micelles (before reconstitution) and in L-α-lecitin vesicles (after reconstitution). Inset shows the absorption and fluorescence spectra (λ_{ex} = 280 nm) of 0.004% TX-114 detergent alone. All samples were measured in 10 mM potassium phosphate buffer, pH 7.2. (C) Recorded UCP2-mediated proton fluxes through L-α-lecitin vesicles in the absence and presence of 100 μM PA. (D) Recorded UCP2-mediated chloride flux through L-α-lecitin vesicles. In both transport assays, the membrane potential was triggerd by the K^+ influxes through K^+-ionophore valinomycin (2 μM). In the chloride transport assays, Cl^- influx quenched SPQ collisionally. In the proton transport assays, fatty acid-activated H^+ effluxes resulted in an increase of TES anions, which quenched SPQ. All UCP2 mutants displayed similar patterns to UCP2-WT in transporting chlorides and protons.

protons across the phospholipid bilayers in the presence of 100 μM LA at comparable transport rates [6−8 μmol min^{-1} (mg of protein)$^{-1}$ or 3−4 protons per second for each UCP2 protein] (Table 2). These rates are within the range of reported proton transport rates for recombinant human UCPs reconstituted in the liposome systems.[10,12,18] In contrast, all UCP2 proteins showed a ~10−60 times lower transport rates in the chloride transport assays, compared to their proton transport rates [~0.1−0.6 μmol min^{-1} (mg of protein)$^{-1}$] (Figure 4, inset). Comparison of the chloride transport rates among UCP2 mutants revealed the basic information about key amino acids in TM2 that are important for the chloride transport activity of UCP2. R96Q and K104Q mutants exhibited similar chloride transport rates to that of UCP2-WT [~0.6 μmol min^{-1} (mg of protein)$^{-1}$] (Figure 4, inset and Table 2). Conversely, R76Q and R88Q mutants showed a 6-fold decrease in chloride transport rates compared to the other versions of the protein (Figure 4, inset). These results indicate that Arg residues at positions 76 and 88 of TM2 play an important role in chloride transport by UCP2.

We also investigated the effect of carbon chain length of FAs on UCP2-mediated proton transport. Three saturated FAs of varying carbon chain lengths were compared as the activators for the UCP2-mediated proton transport: LA (a C12-fatty acid), MA (a C14-fatty acid), and PA (a C16-fatty acid) (Figure 5). As shown in Figure 5 and Table 2, UCP2 and all mutants transported protons at consistently higher rates in the presence of longer chain FAs. In particular, UCP2-WT and its mutants transported protons at rates of 6−8 μmol min^{-1} (mg of protein)$^{-1}$ in the presence of 100 μM LA, 7−19 μmol min^{-1}(mg protein)$^{-1}$ in the presence of 100 μM MA, and 9−21 μmol min^{-1} (mg of protein)$^{-1}$ in the presence of 100 μM PA

DOI: 10.1021/acs.biochem.5b00177
Biochemistry 2015, 54, 2303−2313

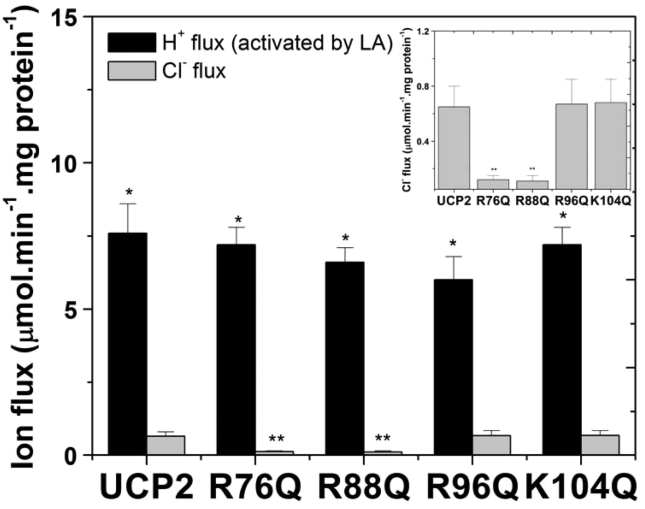

Figure 4. Comparative proton and chloride transport rates of UCP2-WT and its TM2 mutants in liposomes. Results are reported as the average corrected proton and chloride transport rates mediated by UCP2-WT and its TM2 mutants reconstituted in L-α-lecitin vesicles. The reported proton transport rates were calculated in the presence of 100 μM LA activator. Inset shows a comparative chloride transport rates of UCP2-WT and its TM2 mutants. A one-way ANOVA statistical test was performed to determine the statistical significance of the data, and p values were obtained. $p < 0.05$ when comparing the proton transport rates and the chloride transport rates in each protein (*), and $p < 0.05$ when comparing the chloride transport rates of R76Q and R88Q with those mediated by UCP2-WT, R96Q, and K104Q mutants (**).

Table 2. Ion (Proton and Chloride) Transport Rates of UCP2-WT and Mutants in Lipid Vesicles[a]

	ion transport rate [μmol min^{-1} (mg of protein)$^{-1}$]			
protein	H^+ flux (LA activator)	H^+ flux (MA activator)	H^+ flux (PA activator)	Cl^- flux
UCP2 WT	7.6 ± 1	8.5 ± 1	9.2 ± 1	0.65 ± 0.15
UCP2 R76Q	7.2 ± 0.6	8.1 ± 1	9.6 ± 1	0.12 ± 0.03
UCP2 R88Q	6.6 ± 0.5	7.2 ± 0.4	9.7 ± 0.5	0.11 ± 0.04
UCP2 R96Q	6 ± 0.8	11.9 ± 1.6	15.4 ± 1.3	0.67 ± 0.18
UCP2 K104Q	7.2 ± 0.6	19.1 ± 0.8	20.5 ± 1.3	0.68 ± 0.17

[a]The reported rates are the means of 10−20 independent measurements ± the standard errors of the means. The phospholipid concentration was ~20 mg/mL; the final protein content in the liposomes as 2−5 μg/mg of lipid. The final proton transport rates were corrected for the total protein content in the liposomes; the orientations of the reconstituted proteins were ignored in this calculation.

(Table 2). For each FA, the proton transport rate of UCP2-WT and mutants were comparatively analyzed. UCP2-WT and all mutants shared comparable proton transport rates in the presence of the LA activator. On the other hand, differences in proton flux were observed among UCP2 mutants in the presence of longer chain fatty acids, MA and PA. When activated by MA and PA, R96Q and K104Q mutants transported protons at a rate of ~150- 200% higher than all other proteins (Figure 5 and Table 2).

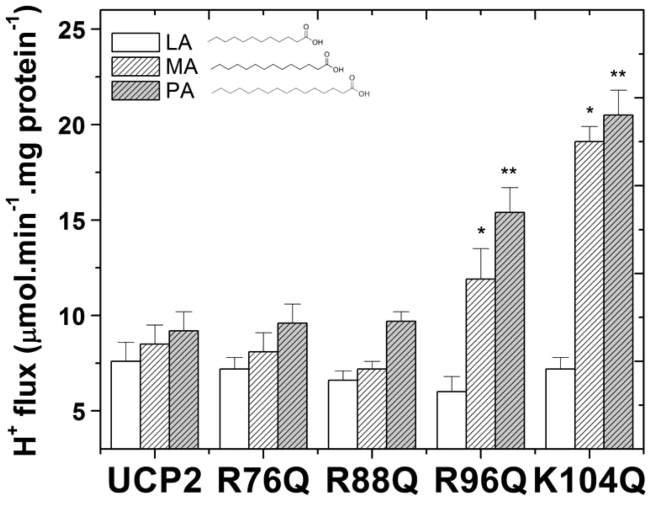

Figure 5. Comparative proton transport rates of UCP2-WT and its TM2 mutants activated by FAs with varying acyl chain lengths. Proton transport rates are reported as the average corrected proton transport rates mediated by UCP2-WT and its TM2 mutants in L-α-lecitin vesicles. The reported proton transport rates were calculated in the presence of 100 μM LA, 100 μM MA, and 100 μM PA activators. A one-way ANOVA statistical test was performed to determine the statistical significance of the data, and p values were obtained. In the presence of 100 μM MA, the proton transport rates of R96Q and K104Q mutants were statistically higher than those of UCP2-WT, R76Q, and R88Q mutants ($p < 0.05$ (*) when comparing H^+ fluxes of R96Q or K104Q mutants to UCP2-WT, R76Q, or R88Q mutant). In the presence of 100 μM PA, the proton transport rates of R96Q and K104Q mutants were also statistically higher than those of UCP2-WT, R76Q, and R88Q mutants ($p < 0.05$ (**) when comparing H^+ fluxes of R96Q or K104Q mutants to UCP2-WT, R76Q, or R88Q mutant).

Comparative Conformations of Reconstituted UCP2-WT and Mutants in Liposomes. The conformations of UCP2-WT and its mutants were compared using the far-UV CD spectra. To maintain a reliable CD signal with a high signal-to-noise ratio, the protein/lipid molar ratio was kept low at ~1:1000, where the reconstituted protein concentrations were ~1−2 μM. As shown in Figure 6A, the far-UV CD spectra of UCP2-WT and its four mutants demonstrated dominant α-helical secondary structures. The proteins' CD spectra contained two minima around 222 and 208 nm, together with a positive local maximum at around 192 nm, which together are characteristic of helical structures (Figure 6A). While sharing a dominantly helical structure, UCP2 and mutants exhibited slight differences in their conformations. R96Q and K104Q mutants' far-UV CD spectra resembled a typical α-helical protein with two minima at 208 and 222 nm (with more intense negative ellipticity at 208 nm) and a positive maximum around 192 nm. The $\theta_{208}/\theta_{222}$ ratios of the R96Q and K104Q mutants' spectra in L-α-lecithin vesicles are above 1 (Figure 6B). On the other hand, UCP2-WT, R76Q, and R88Q mutants exhibited slightly different CD spectra. These spectra possessed the characteristic of an α-helix, with the $\pi \rightarrow \pi^*$ exciton split bands at ~190 and 208 nm and the n $\rightarrow \pi^*$ transition at ~222 nm (Figure 6A). However, compared to a typical α-helical CD spectrum, the parallel band at ~208−210 nm displayed a shoulder-like minimum ellipticity (Figure 6A). The $\theta_{208}/\theta_{222}$ ratios of the UCP2-WT, R76Q, and R88Q spectra in L-α-lecithin vesicles are less than 1 (Figure 6B). As discussed in our previous studies and those of others, a molar ellipticity ratio ($\theta_{208}/\theta_{222}$) of less than 1 often signifies

DOI: 10.1021/acs.biochem.5b00177
Biochemistry 2015, 54, 2303−2313

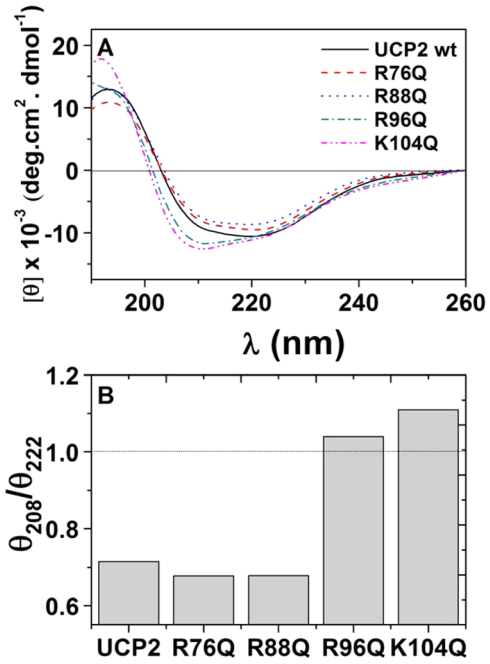

Figure 6. Comparative conformations of UCP2-WT and mutants in phospholipid vesicles. (A) Comparative far-UV CD spectra of reconstituted UCP2-WT and mutants in L-α-lecitin vesicles. Concentrations of proteins and lipids were ~1−2 μM and 1 mM, respectively. All samples were measured in 10 mM potassium phosphate buffer (pH 7.2), using a 0.1 cm path length quartz cuvette. (B) Corresponding $\theta_{208}/\theta_{222}$ plot of reconstituted UCP2-WT and mutants' far-UV CD spectra.

interhelical interactions such as those of coiled-coil motifs and helical TM protein domains and/or association of protein monomers within the membranes.[29−32] Thus, while all reconstituted proteins shared predominantly helical structures in the liposomes, UCP2-WT, -R76Q, and -R88Q mutants exhibited tightly packed conformations, and in comparison, the R96Q and K104Q mutants displayed less compact protein conformations.

DISCUSSION

Chloride Transport of UCP2. Chloride transport activity has been observed for UCP2 and other members of the UCP family.[14−16,18,33] A detailed understanding of the mechanism of chloride transport by UCPs will mark a significant step in understanding the biochemical/physiological role of these proteins in the mitochondria. The results of the current study confirm the importance of positively charged residues in TM2, especially R76 and R88 residues, in the chloride transport activity of UCP2. The R76Q and R88Q mutants of UCP2, while retaining the overall conformation and proton transport function of the UCP2-WT, almost completely lost the ability to transport chloride ions (Figure 4 and Table 2). Our sequence alignment analysis showed that R88 is conserved in all five UCPs (Figure S1, Supporting Information), and thus this residue is expected to play an important role in chloride transport by other UCPs as well. In fact, mutation of this Arg in UCP1 also resulted in a loss in chloride transport but had no impact on its proton transport ability.[8] Compared to UCP2-WT, the two other mutants, R96Q and K104Q, displayed minor conformational differences, but had comparable chloride transport rates (Figure 4 and Table 2). In addition, the chloride transport rates of all UCPs are an order of magnitude lower than those of proton transport rates. This phenomenon has been consistently observed in previous studies.[15,18] Overall, these data provide unambiguous evidence supporting the different mechanisms/pathways for chloride and proton transport activities in UCP2.

In an effort to explain our experimental results, structural characteristics of wild type and mutant forms of UCP2 are compared in Figure 7. The highly positive overall charge of UCP2 (+15), contributed by basic residues Arg and Lys, plays an important role in the overall electrostatic potential of the protein (Figure 7A). This unique electrostatic feature is more or less shared among UCPs and other mitochondrial anion carriers.[18] An analysis of the 3-D molecular structure of UCP2 revealed an accumulation of most of the positively charged residues of the protein located close to the matrix side of the membrane (Figure 7A,B). Among these positively charged residues are R76 and R88, which are crucial in UCP2-mediated chloride transport (Figure 4 and Table 2). Interestingly, molecular dynamic simulation revealed chloride anions to be clustered at the matrix interface of AAC and interact with many basic amino acid residues of the protein.[34] In addition, the AAC charged amino acid residues in the Cl^- binding site are also conserved in UCP2, including D35, K38, R88, D138, K141, K239, and D236 (Figure 7C,D, Figure S1). In this study, mapping of these residues onto the 3D structure of UCP2 revealed a similar positively charged electrostatic pocket to that of AAC close to the protein-matrix interface that could allow for the attraction and transport of chloride anions (Figures 7C,D). Therefore, we suggest that the luminal positive potential of UCP2 plays an important role as a recruiting and transporting site for chloride anions and possibly some other small anions. Consequently, removing any positive charge in this area might impact on the anion transport ability of UCP2. This was evident in the diminished chloride transport rate of R88Q in our study.

At the physiological level, the chloride transport role of UCP2 and other UCPs is not fully understood. While many studies, including this one, have reported a low chloride transport rate for UCPs, evidence of chloride channel activity with a much higher transport rate was obtained for both UCP1 and the TM2 of UCP2.[14,16] Therefore, it is plausible for UCPs to acquire different modes of chloride transport regulated by the variations of membrane potential across the IMM. As discussed in our previous study, the presence of strong luminal positive potential and the water accessibility from both sides of UCP2 (Figure 7) can generate a potential-sensitive charged area that could attract small anions.[18] The accumulation of these small anions at the protein−matrix interface can lower the membrane potential at this interface, inducing conformational changes in the protein. It is plausible that the lowering of interface membrane potential, together with the conformational change of UCP2, can cause the formation of transient channel-like openings to allow anion flux across the membrane. It is also worth mentioning that in the IMM, there are also other mitochondrial chloride channels including IMAC and CLCs.[35] Currently, it is speculated that these mitochondrial chloride channels are involved in the volume and potential regulation in mitochondria.[35]

FA-Activated Proton Transport of UCP2. Although the FA-activated proton transport of UCP2 and other UCPs has been confirmed, the mechanism of this activation is still debated. In this study, we were able to differentiate the proton

DOI: 10.1021/acs.biochem.5b00177
Biochemistry 2015, 54, 2303−2313

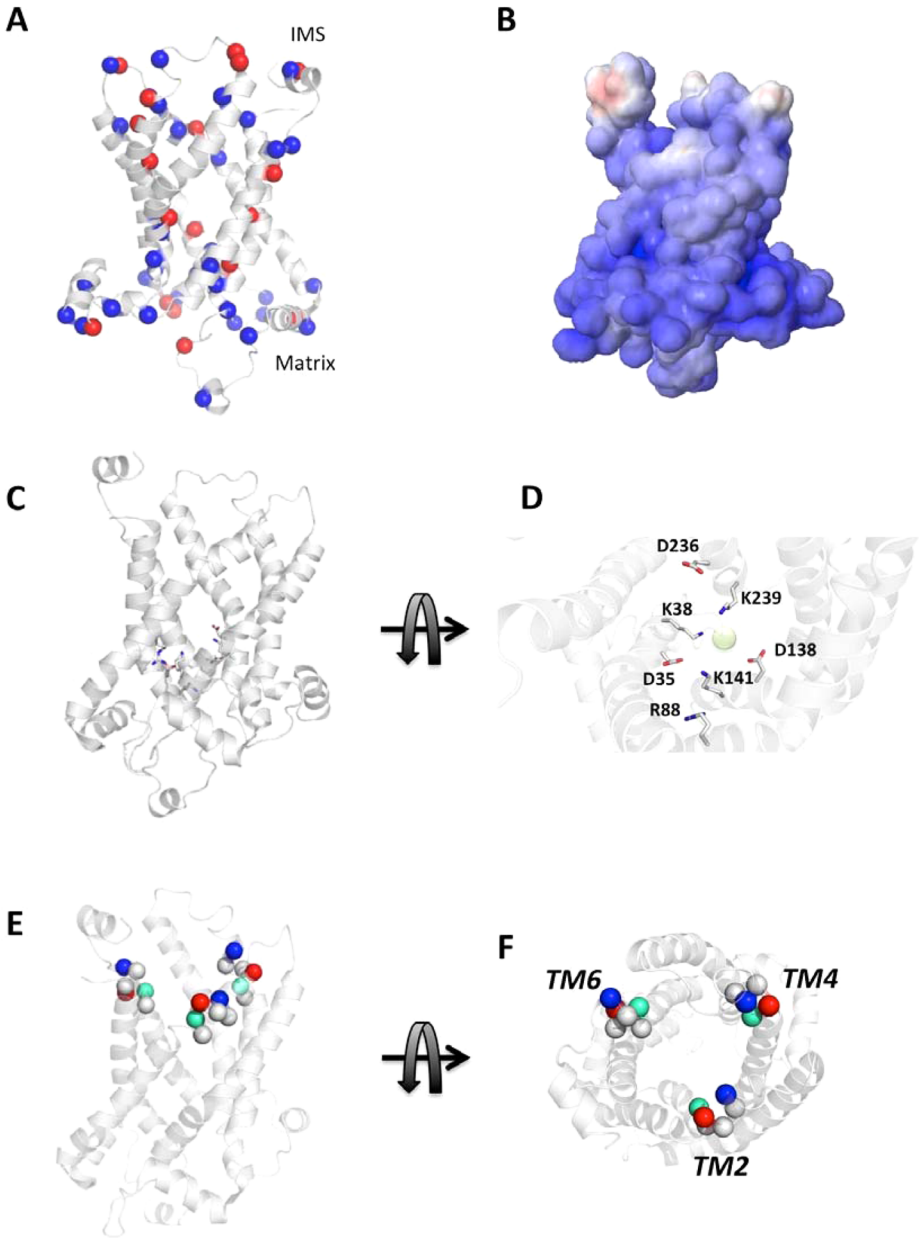

Figure 7. Detailed structural analysis of UCP2. (A) Spatial distribution of positively charged residues (blue balls) and negatively charged residues (red balls) in UCP2. (B) Electrostatic potential of UCP2, calculated by using the nonlinear Poisson−Boltzmann equation, is displayed at a contour level of ±10kT. The electrostatic potential is represented in a color spectrum from red (for negative potential) to blue (for positive potential). (C, D) Conserved amino acid residues that have been predicted to participate in the chloride transport of UCP2, similarly to that of AAC, are highlighted. Chloride anion is represented as a green sphere. (E, F) Conserved [Y/F][D/E]xx[K/R] motif in the cytoplasmic salt-bridge network on TMs 2, 4, and 6 of UCP2. Positively charged residues are represented as blue balls, while negatively charged residues are represented as red balls and other residues are shown as cyan balls.

and small anion transport pathways (Figure 4 and Table 2). As previously mentioned, R76 and R88 are crucial for chloride transport, while R96 and K104 are important for the overall structure of UCP2 and consequently play a role in the proton transport rate of the protein. In addition, our results implicate the importance of hydrophobic interactions between UCP2 and proton transport activator FAs. Across all UCP2 mutants, longer carbon chain-length FAs induced stronger proton transport rates (Figure 5). Therefore, the FA-UCP hydrophobic interactions play an important role in activating the proton transport in UCP2. The role of hydrophobic interactions in the binding of FAs to UCP1 coupled with H^+ transport has also been emphasized in a patch clamp study of UCP1.[15] In that study, it has been suggested that in the case of short-chain low-pK_a FA analogues, FA-UCP1 hydrophobic interactions could not be established and the FAs can dissociate from UCP1 without transporting H^+. On the other hand, as the carbon chain-length of FAs increases, the FA-UCP1 hydrophobic interaction could facilitate the coupling of proton transport through UCP1.[15] In one of our recent studies, UCP2, UCP4, and UCP5 transported protons in the presence of FAs with long carbon chains (C > 12), while they did not transport protons in the presence of succinic acid (Hoang T., Smith M. D., Jelokhani-Niaraki M, unpublished data). On the basis of these findings, a possibility for a specific hydrophobic pocket in UCP2 for FA binding cannot be excluded and even seems

DOI: 10.1021/acs.biochem.5b00177
Biochemistry 2015, 54, 2303−2313

plausible. Phospholipids contain hydrocarbon chains with comparable length to long-chain FAs, and therefore specific phospholipid−UCP interactions could provide extra information on the binding between FAs and UCPs. The recent crystal structures of AAC revealed a strong interaction of the protein with mitochondrial phospholipid cardiolipin (CL).[36−38] Multiple sequence alignment revealed that many amino acid residues in the CL-AAC interaction sites are conserved in UCP2 and other UCPs (Figure S1). It is important to note that our previous studies also demonstrated a direct modulation of CL on UCPs' structure and function.[18,29]

An important observation in the current study is the relationship between the structure and proton transport activity of UCP2. The mutation at the two positively charged residues close to the intermembrane side (R96 and K104) induced a change in the secondary structure of reconstituted UCP2 and increased its helicity (Figure 6). Compared to UCP2-WT and the other two mutants (R76Q and R88Q), both R96Q and K104Q, exhibited interhelical packing that was not as tight, and a more relaxed overall conformation (Figure 6). This more relaxed conformation of UCP2 correlated with a higher rate of proton transport in the presence of MA and PA (Figure 5 and Table 2). It is important to note that the dense packing phenomenon has been observed in all crystal structures of AACs.[37,38] It has been proposed that AACs and other MCF proteins might experience superpacking in the inner membrane of mitochondria.[37] The mitochondrial lipid CL has been suggested to release the stress of protein packing and modulate the ion transport of MCF proteins.[18,29,39−41] In a previous study, we also observed the cardiolipin-induced relaxed conformation in UCP1, together with an increased proton transport rate of the protein.[29] We therefore suggest that R96 and K104 can participate in protein−protein interactions of UCP2, and the effects of the mutations at these two residues could be due to disruption of intermolecular interactions resulting in a less densely packed protein that in turn increases the rate of proton transport. To further explore this hypothesis, we performed a detailed sequence analysis and sequence alignment of UCPs and AACs, which revealed the participation of K104 in a conserved motif [Y/F][D/E]xx[K/R] (Figure 7E,F, Figure S1).[42] Existing on the cytoplasmic side of the even-numbered TMs (TM-2, -4, and -6) of AAC, these motifs were suggested to form a salt-bridge network.[42] It has also been proposed that the interaction between positively and negatively charged residues in this cytoplasmic interface of the protein can restrict movement in TMs during substrate transport by AAC.[42] The arrangement of this motif was similarly observed in the 3-D structure of UCP2, where the conserved [Y/F][D/E]xx[K/R] on TM-2, -4, and -6 line up at the water−membrane interface of the protein close to the cytoplasm (Figure 7E,F). The electrostatic interaction of oppositely charged residues between adjacent TMs could play an important role in the cytoplasmic salt-bridge network formation of UCP2 (Figure 7F). K104 is located on TM2 and is likely to interact electrostatically with the negatively charged D198 on TM4. Therefore, elimination of the positively charged Lys at this position could result in disruption of the charge−charge interaction in the cytoplasmic salt-bridge network. In addition, a sequence analysis of UCP2 revealed three conserved GxxxG motifs that are commonly found in TM helix−helix association (Figure S1).[43] One of the motifs is located on TM2 close to the mentioned cytoplasmic salt-bridge network. Therefore, disruption of the salt-bridge network or any residue in this vicinity could alter the amino acid interaction (electrostatic, H bonding, or van der Waals) that induces a change in the protein conformation and transport activity. Taking the experimental results and the structural analysis of UCP2 into account, we propose that the mutations of the positively charged residues (R96 and K104) on TM2 induced the relaxed conformations of R96Q and K104Q mutants. These protein conformations allowed a better hydrophobic interaction of UCP2 with FAs (MA and PA), resulting in a more efficient activation and faster proton transport.

CONCLUSIONS

Overall, our experimental results highlight the role of positively charged residues in TM2 of UCP2 in the protein's ion transport pathway. A complete picture of the ion transport mechanism of UCP2 can be drawn from future work on other TMs of the protein. Interestingly, in a recent study using hepatocarcinoma cells, it has been suggested that UCP2 can act as a transporter to catalyze the transport of specific C4 metabolites (malate, oxaloacetate, and aspartate) out of the mitochondrial inner membrane in exchange for inward transport of phosphate and proton ions, regulating glucose and glutamine oxidation in the cells.[44] The exchange C4/phosphate-proton transport by UCP2 was inhibited by purine nucleotides but not by LA. This recent report implies that UCP2 could possess different modes of ion transport functions under different physiological conditions. There is ample evidence in the literature for membrane proteins with structural polymorphism and multifunctionality.[45−47] For example, in previous studies it has been shown that ADP/ATP carrier can also transport H^+ under the influence of FAs.[48] Therefore, the finding that UCP2 functions as an exchange transporter is intriguing, but does not exclude the protein's role as a proton transporter under the influence of fatty acids, or its role as small anion (chloride) transporter under different physiological conditions. It is worth mentioning that neither chloride transport nor fatty acid activation of proton transport of UCP2 was examined in this recent study.[44] In a complementary study, we have examined the effect of a citric acid cycle C4 metabolite, succinic acid, on the proton transport activities of UCP2 and other neuronal UCPs 4 and 5. In this study, succinic acid did not activate proton transport of UCP2 or other neuronal UCPs (Hoang, T., Smith, M., and Jelokhani-Niaraki, M., unpublished results). The succinic acid-activated proton transport by UCP2 may require an addition of phosphate anions,[44] but further experimentation is required for its verification. As two positively charged residues of UCP2 at the mitochondrial matrix−protein interface (R76 and R88) play an important role in the protein-mediated anion transport, mutating these two residues might also affect the transport of C4 metabolites of the protein, as these metabolites are negatively charged at physiological pH. This will be an interesting possibility to test in the future but is outside the scope of the current study.

At the moment, UCP2 remains a potential therapeutic target due to its expression in different human tissues. There is strong evidence that UCP2-mediated proton transport activity attenuates mitochondrial ROS production.[3,6] This function leads to a protective role for UCP2 in many cells, including neurons and β-cells. The flexibility of activating UCP2-mediated proton transport by various types of FAs and other derivatives could highlight a regulatory role for the protein. Clarifying the mechanism of proton transport activation by FAs

DOI: 10.1021/acs.biochem.5b00177
Biochemistry 2015, 54, 2303−2313

is a necessary step toward a better understanding of the biochemical and physiological roles of UCP2. Recent studies reported a high proton transport rate of UCP2 in the presence of polyunsaturated FAs (e.g., linoleic acids, arachidonic acids).[49] In addition, long chain FAs generated from the IMM were observed to activate the proton flux mediated by UCP1.[15] Thus, it is plausible that the FAs generated within the IMM under different physiological conditions might serve as activators and regulators of the mitochondrial UCP2.

■ ASSOCIATED CONTENT

Supporting Information

Sequence alignment results for five human UCPs and ADP/ATP carrier. This material is available free of charge via the Internet at http://pubs.acs.org.

■ AUTHOR INFORMATION

Corresponding Author

*Address: Department of Chemistry and Biochemistry, Wilfrid Laurier University, 75 University Avenue West, Waterloo, ON, N2L 3C5, Canada. Tel: +1-(519)-884-0710 ext 2284. Fax: +1-(519)-746-0677. E-mail: mjelokhani@wlu.ca.

Funding

This research was supported by grants from the Canada Foundation for Innovation (CFI) and the Natural Sciences and Engineering Research Council of Canada (NSERC) to M.J.N. (CFI, 6786; NSERC, 250119) and M.D.S. (CFI, 11292; NSERC, 312143). T.H. has been a recipient of NSERC CGS Doctoral and OGS scholarships.

Notes

The authors declare no competing financial interest.

■ ACKNOWLEDGMENTS

We thank Tyler Auld, Wilfrid Laurier University, for technical support.

■ ABBREVIATIONS

AAC, ADP/ATP carrier; BAT, brown adipose tissue; CAPS, *N*-cyclohexyl-3-aminopropanesulfonic acid; CD, circular dichroism; CL, cardiolipin; C_8E_4, octyltetraoxyethylene; EtBr, ethidium bromide; FA, fatty acid; IMM, inner mitochondrial membrane; IPTG, isopropyl-β-thiogalactopyranoside; LA, lauric acid; LDAO, lauryldimethylamine-oxide; MA, myristic acid; MCF, mitochondrial carrier family; PA, palmitic acid; PCR, polymerase chain reaction; ROS, reactive oxygen species; SDS, sodium dodecyl sulfate; SPQ, 6-methoxy-*N*-(3-sulfopropyl)quinolinium; TBS, Tris-buffered-saline; TEA, tetraethylammonium; TES, *N*-[tris(hydroxymethyl)methyl]-2-aminoethane-sulfonic acid; TM, transmembrane; TX-100, octyl phenol ethoxylate; TX-114, polyethylene glycol *tert*-octylphenyl ether; UCP, uncoupling protein

■ REFERENCES

(1) Krauss, S., Zhang, C. Y., and Lowell, B. B. (2005) The mitochondrial uncoupling protein homologs. *Nat. Rev. Mol. Cell Biol. 6*, 248−261.

(2) Echtay, K. S. (2007) Mitochondrial uncoupling proteins − what is their physiological role? *Free Radical Biol. Med. 43*, 1351−1371.

(3) Andrews, Z. B., Diano, S., and Horvath, T. L. (2005) Mitochondrial uncoupling proteins in the CNS: in support of function and survival. *Nat. Rev. Neurosci. 6*, 829−840.

(4) Nicholls, D. G., Bernson, V. S., and Heaton, G. M. (1978) The identification of the component in the inner membrane of brown adipose tissue mitochondria responsible for regulating energy dissipation. *Exp. Suppl. 32*, 89−93.

(5) Echtay, K. S., Winkler, E., Frischmuth, K., and Klingenberg, M. (2001) Uncoupling proteins 2 and 3 are highly active H^+ transporters and highly nucleotide sensitive when activated by coenzyme Q (ubiquinone). *Proc. Natl. Acad. Sci. U.S.A. 98*, 1416−1421.

(6) Echtay, K. S., Roussel, D., St-Pierre, J., Jekabsons, M. B., Cadenas, S., Stuart, J. A., Harper, J. A., Roebuck, S. J., Morrison, A., Pickering, S., Clapham, J. C., and Brand, M. D. (2002) Superoxide activates mitochondrial uncoupling proteins. *Nature 415*, 96−99.

(7) Chan, C. B., De Leo, D., Joseph, J. W., McQuaid, T. S., Ha, X. F., Xu, F., Tsushima, R. G., Pennefather, P. S., Salapatek, A. M., and Wheeler, M. B. (2001) Increased uncoupling protein-2 levels in beta-cells are associated with impaired glucose-stimulated insulin secretion: mechanism of action. *Diabetes 50*, 1302−1310.

(8) Klingenberg, M., and Echtay, K. S. (2001) Uncoupling proteins: the issues from a biochemist point of view. *Biochim. Biophys. Acta 1504*, 128−143.

(9) Berardi, M. J., Shih, W. M., Harrison, S. C., and Chou, J. J. (2011) Mitochondrial uncoupling protein 2 structure determined by NMR molecular fragment searching. *Nature 476*, 109−113.

(10) Jabůrek, M., and Garlid, K. D. (2003) Reconstitution of recombinant uncoupling proteins UCP1, −2, and −3 have similar affinities for ATP and are unaffected by coenzyme Q10. *J. Biol. Chem. 278*, 25825−25831.

(11) Garlid, K. D., Orosz, D. E., Modriansky, M., Vassanelli, S., and Jezek, P. (1996) On the mechanism of fatty acid-induced proton transport by mitochondrial uncoupling protein. *J. Biol. Chem. 271*, 2615−2620.

(12) Echtay, K. S., Winkler, E., Bienengraeber, M., and Klingenberg, M. (2000) Site-directed mutagenesis identifies residues in uncoupling protein (UCP1) involved in three different functions. *Biochemistry 39*, 3311−3317.

(13) Echtay, K. S., Bienengraeber, M., and Klingenberg, M. (2001) Role of intrahelical arginine residues in functional properties of uncoupling protein (UCP1). *Biochemistry 40*, 5243−5248.

(14) Huang, S. G., and Klingenberg, M. (1996) Chloride channel properties of the uncoupling protein from brown adipose tissue mitochondria: a patch-clamp study. *Biochemistry 35*, 16806−16814.

(15) Fedorenko, A., Lishko, P. V., and Kirichok, Y. (2012) Mechanism of fatty-acid-dependent UCP1 uncoupling in brown fat mitochondria. *Cell 151*, 400−413.

(16) Yamaguchi, H., Jelokhani-Niaraki, M., and Kodama, H. (2004) Second transmembrane domain of human uncoupling protein 2 is essential for its anion channel formation. *FEBS Lett. 577*, 299−304.

(17) Heckman, K. L., and Pease, L. R. (2007) Gene splicing and mutagenesis by PCR-driven overlap extension. *Nat. Protoc. 2*, 924−932.

(18) Hoang, T., Smith, M. D., and Jelokhani-Niaraki, M. (2012) Toward understanding the mechanism of ion transport activity of neuronal uncoupling proteins UCP2, UCP4, and UCP5. *Biochemistry 51*, 4004−4014.

(19) Whitmore, L., and Wallace, B. A. (2004) DICHROWEB, an online server for protein secondary structure analyses from circular dichroism spectroscopic data. *Nucleic Acids Res. 32*, W668−673.

(20) Lees, J. G., Miles, A. J., Wien, F., and Wallace, B. A. (2006) A reference database for circular dichroism spectroscopy covering fold and secondary structure space. *Bioinformatics. 22*, 1955−1962.

(21) Sievers, F., Wilm, A., Dineen, D., Gibson, T. J., Karplus, K., Li, W., Lopez, R., McWilliam, H., Remmert, M., Söding, J., Thompson, J. D., and Higgins, D. G. (2011) Fast, scalable generation of high-quality protein multiple sequence alignments using Clustal Omega. *Mol. Syst. Biol. 7*, 539.

(22) Waterhouse, A. M., Procter, J. B., Martin, D. M. A., Clamp, M., and Barton, G. J. (2009) Jalview Version 2—a multiple sequence alignment editor and analysis workbench. *Bioinformatics 25*, 1189−1191.

(23) DeLano, W. L. (2002) *PyMOL*; DeLano Scientific, San Carlos, CA.

DOI: 10.1021/acs.biochem.5b00177
Biochemistry 2015, 54, 2303−2313

(24) Dolinsky, T. J., Czodrowski, P., Li, H., Nielsen, J. E., Jensen, J. H., Klebe, G., and Baker, N. A. (2007) PDB2PQR: expanding and upgrading automated preparation of biomolecular structures for molecular simulations. *Nucleic Acids Res. 35*, W522−525.
(25) Dolinsky, T. J., Nielsen, J. E., McCammon, J. A., and Baker, N. A. (2004) PDB2PQR: an automated pipeline for the setup of Poisson−Boltzmann electrostatics calculations. *Nucleic Acids Res. 32*, W665−667.
(26) Baker, N. A., Sept, D., Joseph, S., Holst, M. J., and McCammon, J. A. (2001) Electrostatics of nanosystems: Application to microtubules and the ribosome. *Proc. Natl. Acad. Sci. U. S. A. 98*, 10037−10041.
(27) Mao, D., and Wallace, B. A. (1984) Differential light scattering and absorption flattening optical effects are minimal in the circular dichroism spectra of small unilamellar vesicles. *Biochemistry 23*, 2667−2673.
(28) Ivanova, M. V., Hoang, T., McSorley, F. R., Krnac, G., Smith, M. D., and Jelokhani-Niaraki, M. (2009) A comparative study on conformation and ligand binding of the neuronal uncoupling proteins. *Biochemistry 49*, 512−521.
(29) Hoang, T., Smith, M. D., and Jelokhani-Niaraki, M. (2013) Expression, folding and proton transport activity of human uncoupling protein-1 (UCP1) in lipid membranes: evidence for associated functional forms. *J. Biol. Chem. 288*, 36244−36258.
(30) Greenfield, N. J., and Hitchcock-DeGregori, S. E. (1993) Conformational intermediates in the folding of a coiled-coil model peptide of the N-terminus of tropomyosin and alpha alpha-tropomyosin. *Protein Sci. 2*, 1263−1273.
(31) Cooper, T. M., and Woody, R. W. (1990) The effect of conformation on the CD of interacting helices: a theoretical study of tropomyosin. *Biopolymers 30*, 657−676.
(32) Salom, D., Hill, B. R., Lear, J. D., and DeGrado, W. F. (2000) pH-dependent tetramerization and amantadine binding of the transmembrane helix of M2 from the influenza A virus. *Biochemistry 39*, 14160−14170.
(33) Echtay, K. S., Liu, Q., Caskey, T., Winkler, E., Frischmuth, K., Bienengräber, M., and Klingenberg, M. (1999) Regulation of UCP3 by nucleotides is different from regulation of UCP1. *FEBS Lett. 450*, 8−12.
(34) Wang, Y., and Tajkhorshid, E. (2008) Electrostatic funneling of substrate in mitochondrial inner membrane carriers. *Proc. Natl. Acad. Sci. U. S. A. 105*, 9598−9603.
(35) Tomaskova, Z., and Ondrias, K. (2010) Mitochondrial chloride channels − What are they for? *FEBS Lett. 584*, 2085−2092.
(36) Pebay-Peyroula, E., Dahout-Gonzalez, C., Kahn, R., Trézéguet, V., Lauquin, G. J. M., and Brandolin, G. (2003) Structure of mitochondrial ADP/ATP carrier in complex with carboxyatractyloside. *Nature 426*, 39−44.
(37) Nury, H., Dahout-Gonzalez, C., Trézéguet, V., Lauquin, G., Brandolin, G., and Pebay-Peyroula, E. (2005) Structural basis for lipid-mediated interactions between mitochondrial ADP/ATP carrier monomers. *FEBS Lett. 579*, 6031−6036.
(38) Ruprecht, J. J., Hellawell, A. M., Harding, M., Crichton, P. G., McCoy, A. J., and Kunji, E. R. S. (2014) Structures of yeast mitochondrial ADP/ATP carriers support a domain-based alternating-access transport mechanism. *Proc. Natl. Acad. Sci. U. S. A. 111*, 426−434.
(39) Kadenbach, B., Mende, P., Kolbe, H. V., Stipani, I., and Palmieri, F. (1982) The mitochondrial phosphate carrier has an essential requirement for cardiolipin. *FEBS Lett. 139*, 109−112.
(40) Pfeiffer, K., Gohil, V., Stuart, R. A., Hunte, C., Brandt, U., Greenberg, M. L., and Schägger, H. (2003) Cardiolipin stabilizes respiratory chain supercomplexes. *J. Biol. Chem. 278*, 52873−52880.
(41) Renner, L. D., and Weibel, D. B. (2011) Cardiolipin microdomains localize to negatively curved regions of Escherichia coli membranes. *Proc. Natl. Acad. Sci. U. S. A. 108*, 6264−6269.
(42) Robinson, A. J., Overy, C., and Kunji, E. R. S. (2008) The mechanism of transport by mitochondrial carriers based on analysis of symmetry. *Proc. Natl. Acad. Sci. U. S. A. 105*, 17766−17771.
(43) Russ, W. P., and Engelman, D. M. (2000) The GxxxG motif: a framework for transmembrane helix-helix association. *J. Mol. Biol. 296*, 911−919.
(44) Vozza, A., Parisi, G., De Leonardis, F., Lasorsa, F. M., Castegna, A., Amorese, D., Marmo, R., Calcagnile, V. M., Palmieri, L., Ricquier, D., Paradies, E., Scarcia, P., Palmieri, F., Bouillaud, F., and Fiermonte, G. (2014) UCP2 transports C4 metabolites out of mitochondria, regulating glucose and glutamine oxidation. *Proc. Natl. Acad. Sci. U. S. A. 111*, 960−965.
(45) Harauz, G., Ladizhansky, V., and Boggs, J. M. (2009) Structural polymorphism and multifunctionality of myelin basic protein. *Biochemistry 48*, 8094−8104.
(46) Werner, J., Augustus, A. M., and Misra, R. (2003) Assembly of TolC, a structurally unique and multifunctional outer membrane protein of *Escherichia coli* K-12. *J. Bacteriol. 185*, 6540−6547.
(47) Laus, M. N., Soccio, M., Trono, D., Cattivelli, L., and Pastore, D. (2008) Plant inner membrane anion channel (PIMAC) function in plant mitochondria. *Plant Cell Physiol. 49*, 1039−1055.
(48) Brustovetsky, N., and Klingenberg, M. (1994) The reconstituted ADP/ATP carrier can mediate H^+ transport by free fatty acids, which is further stimulated by mersalyl. *J. Biol. Chem. 269*, 27329−27336.
(49) Beck, V., Jaburek, M., Demina, T., Rupprecht, A., Porter, R. K., Ježek, P., and Pohl, E. E. (2007) Polyunsaturated fatty acids activate human uncoupling proteins 1 and 2 in planar lipid bilayers. *FASEB J. 21*, 1137−1144.

DOI: 10.1021/acs.biochem.5b00177
Biochemistry 2015, 54, 2303−2313